Homogeneous phase separation in binary alloys under ion irradiation conditions: Role of interstitial atoms

P. Krasnochtchekov, R. S. Averback, and P. Bellon
Department of Materials Science and Engineering, University of Illinois at Urbana-Champaign, Urbana, Illinois 61801, USA
(Received 4 December 2006; published 20 April 2007)

Kinetic Monte Carlo simulations have been performed to investigate homogeneous precipitation in binary metal alloys under ion irradiation conditions. The kinetic model includes defect production, recombination, defect trapping, the formation of defect-solute complexes, and atomic mixing. While no special assumptions are made about vacancy diffusion, interstitial diffusion is assumed fast compared to the characteristic time scales of all other processes. The diffusion path of an interstitial, moreover, ends with one of the three possible outcomes: recombination, trapping in a solute-rich location, or clustering with other interstitials. Interstitials promote solute segregation in this model by the formation of mobile interstitial-solute complexes. Several unusual features of radiation-induced precipitation are revealed in this model. For ideal alloys, we find at a given temperature that for every trapping number [i.e., the minimum number of nearest-neighbor solute (type B) atoms required to trap a migrating interstitial, N_{BT}], there exists a corresponding defect pair production rate K_0, below which the alloy becomes a random solution state and above which macroscopic phase separation occurs. K_0 depends on the length scale of trapping sites L as L^4. Solute-rich precipitates have the composition c_B approaching $c_B=N_{BT}/z$, where z is the lattice coordination number. This feature results in "swelling" of precipitates, i.e., dilution of initially pure ($c_B=1$) precipitates located in the matrix prior to ion irradiation. Ballistic mixing is observed to erode precipitates, and above some critical rate the system reverts to a random solution. For ideal solutions, and even those with a small tendency for ordering, phase separation occurs due to the interstitial interaction with solutes. At sufficiently high positive values of the heats of mixing, the usual thermal vacancy-driven precipitation prevails. Between these low and high limits, the alloy unexpectedly enters a field of solid solutions. Finally, it is shown that even in the absence of the interstitial trapping ($N_{BT}>z$), alloys with a small positive ordering energy can undergo nonequilibrium phase separation at a composition below its solubility limit due to an effective trapping of vacancies in solute-rich locations. The significance of these findings for real alloy systems is discussed.

DOI: 10.1103/PhysRevB.75.144107 PACS number(s): 61.80.−x, 61.72.Ji, 64.75.+g, 61.82.Bg

I. INTRODUCTION

While thermal aging of binary alloys is now understood in some detail, phase stability and kinetic behavior in alloys under ion irradiation remain a challenging problem despite years of investigation.[1] The difficulty, as long appreciated, arises because irradiation drives alloy system far from equilibrium, so that kinetic factors, rather than thermodynamics, often control the steady-state morphology. The defining features of ion irradiation are the production of large supersaturations of Frenkel pairs (vacancies and interstitials) and the athermal mixing of atoms (ballistic mixing) in the defect production process. Since defects are produced in pairs, phase separation in irradiated alloys depends on the properties of both interstitial and vacancy defects.

Past studies on closed systems, i.e., systems with conserved point defects, showed that changes in free energies of alloy phases caused by the presence of point defects are not sufficiently large to induce phase separation, even at very high defect concentrations.[2,3] Thus, point defect annihilation at external or internal sinks or recombination of defect pairs in the bulk is thought to lie at the origin of the radiation-induced precipitation (RIP). Solute precipitation on preexisting sinks (e.g., surfaces, grain boundaries, and dislocation cores) corresponds to heterogeneous nucleation, while precipitation in the bulk, due to defect recombination, corresponds to homogeneous nucleation. Examples of heterogeneous nucleation at sinks are reported in such systems as Ni-Si (Refs. 4 and 5) and Ni-Be (Ref. 6), as well as steels with Ni and Si impurities,[7] while homogeneous nucleation was suggested for AlZn (Ref. 8) and CuNi (Ref. 9) alloys. Obviously, the necessary condition for heterogeneous nucleation is the coupling between the fluxes of point defects and solute atoms. Both vacancies and interstitials are capable of transporting solute atoms, either directly through preferential exchanges with solute atoms or by carrying solute atoms as a part of a bound defect complex.[7,10,11] Several numerical models based on the solution of diffusion equations with coupled fluxes were used in the past to account for the observed heterogeneous RIP effects.[12] More recently, Soisson has employed kinetic Monte Carlo (KMC) simulations to examine solute segregation at dislocations and grain boundaries in irradiated alloys.[13] These simulations include both vacancy and interstitial defects, but not ballistic events.

For homogeneous nucleation, an additional condition of trapping of one type of defect at the locations with high solute concentration is obviously required.[8] Statistical fluctuations in the local density of solute concentration, therefore, can lead to a preferential trapping of one type of point defect, increasing the probability of recombination at these locations. If one of the defect species is likely to drag a solute atom along with it, a self-sustaining deposition of solute atoms at these locations may lead to nucleation and growth of the solute-rich phase. In thermodynamically ran-

dom solutions, however, this growth mechanism is countered by the randomizing action of the point defects, typically the vacancies. The present study focuses on homogeneous phase separation under irradiation, specifically examining the conditions establishing the boundary between the regimes of random solution and phase separation as well as the morphologies and microstructures of the thus-formed precipitates.

The possibility for homogeneous nucleation of precipitates in irradiated alloys was previously considered theoretically by Martin and co-worker.[14,15] In Ref. 14, for example, Martin performed a linear stability analysis for a general set of differential equations balancing the fluxes of interstitials, vacancies, and solute atoms in the irradiated alloy. The present work expands on this formal treatment by developing a specific model of an alloy and exploring the consequences through KMC simulation.

We assume in our KMC model strong coupling between interstitials and solute. Interactions of the interstitials with solute atoms have, in fact, long been studied. These studies have shown, for example, that interstitials are capable of capturing solute atoms in solution and carrying them to sinks, such as the grain boundaries, resulting in segregation and precipitation.[16] Interstitials are also known to form immobile clusters which, at large sizes, become two-dimensional platelets or dislocation loops. An additional parameter describing interstitial interactions with the solute atoms, and significant for the present work, is the trapping number N_{BT}, i.e., the minimum number of first-neighbor solute atoms required to trap a solute-type interstitial. It has been shown, for example, that interstitial-solute complexes in Ni-1 at. % Si alloys are nearly as mobile as self-interstitials, but that they become trapped if additional solute atoms are present.[17] Based on these prominent features of interstitial properties in alloys, i.e., a small migration energy (relative to vacancies), a tendency to form bound complexes with solute atoms, the formation of immobile interstitial clusters, and trapping in solute-rich locations, a simple set of rules can be devised to investigate the role that interstitials can play in the homogeneous precipitation of irradiated alloys. While most of the simulations described here refer to ideal solid solutions to focus directly on the effects of the interstitials, phase separation in more complex alloys, with competing vacancy-driven and interstitial-driven mechanisms of precipitation, is also addressed. We also consider ballistic mixing in this process.

II. COMPUTATIONAL METHOD

The KMC code used in this work is based on the single-vacancy code used in earlier studies.[18] A model fcc A-B binary alloy is defined in KMC simulations by the pure A and B cohesive energies ($E_C^A = z/2\varepsilon_{AA}$ and $E_C^B = z/2\varepsilon_{BB}$), vacancy formation energies $E_V^{A,F}$ and $E_V^{B,F}$, and the ordering energy $\omega = 2\varepsilon_{AB} - \varepsilon_{AA} - \varepsilon_{BB}$ (ε_{XY} are X-Y bond energies). The following values were used for these parameters for the A-B system with zero ordering energy: $E_C^A = E_C^B = -4.340$ eV, $E_V^{A,F} = E_V^{B,F} = 1.28$ eV, and $\omega = 0$. The simulations were all performed at temperature $k_B T = 0.040\,76$ eV ($T = 200$ °C). The vacancy migration energy E_V^M was set at $E_V^M = 0.80$ eV. The frequency of vacancy jumps in the prefactor, ν_0, was $\nu_0 = 10^{14}$ s^{-1}. Simulations reported in this study were performed on $A_{0.90}B_{0.10}$ systems in rhombohedral simulation volumes of sizes 128^3 and 64^3 atomic volumes, and with periodic boundary conditions. The code has been modified to include multiple defects of both types. Frenkel pairs were randomly produced in isolation at a given rate K_0. Each pair was created by selecting a lattice site and moving the resident atom to one of the six second-nearest-neighbor sites. An interstitial was thus created a distance a_o (lattice constant) from the vacancy. As such, every interstitial atom is assigned to a lattice point.

Vacancies follow the same jump rules as in previous KMC simulations,[18] although for simplicity we prohibited their clustering by adding a small repulsive interaction between vacancies. When a vacancy encounters an interstitial (and vice versa) within its recombination volume, a recombination event is recorded. The recombination radius is set at the first-nearest-neighbor distance a_{nn}; this results in a "correlated" recombination rate of $\approx 70\%$. Interstitial motion is governed by a set of simple rules. Once generated, an interstitial travels until it recombines with a vacancy, becomes trapped in a solute-rich neighborhood, or forms an immobile cluster with another interstitial or a group of interstitials. The motion of interstitials is assumed much faster than that of vacancies and is thus considered to be instantaneous. When trapped, interstitials remain immobile until the local environment changes to affect their recombination or set them in motion again. Interstitials diffuse in a biased random-walk pattern with a preference for jumps to B-atom sites among their nearest neighbors. Both A- and B-type interstitials are allowed in the simulations; however, there is a provision that A-type interstitials convert to B-type interstitials upon their first jump to a B-type lattice atom by switching the interstitial and lattice atom types. We also impose a condition for the probability, P_A, for B-type interstitials to jump to any of its A-atom-type neighbor sites:

$$P_A = 0.5\frac{N_{BT} - N_B}{N_{BT} - 1}, \tag{1}$$

where N_B is the number of nearest-neighbor B atoms and N_{BT} is the number of nearest-neighbor B atoms required for trapping. Thus, when there is a single B atom in the neighborhood of a B interstitial, the interstitial according to Eq. (1) has equal chance to jump to this B site or to any one of the remaining 11 A sites. As the number of B neighbors increases, the relative probability of jumps to A neighbors decreases until it vanishes at $N_B = N_{BT}$. At this number of B-type neighbors, a B-type interstitial is considered to be permanently immobilized and is denoted as B trapped. It should be noted that the nonzero probability of interstitial jumps to A-type sites for $N_B < N_{BT}$ is needed to ensure that an interstitial can always escape from any environment with N_B fewer than N_{BT}. Other methods to prevent interstitial trapping at N_B values less than N_{BT} were also tried, but with little effect on the results. Interstitial clustering of both A- and B-type interstitials is allowed in these simulations, with the

capture radii equal to the second-nearest-neighbor distance. It should be noted that within the assumption of infinitely fast interstitial diffusion, no more than one interstitial is in motion at any time in the simulation volume. Thus, a single *B*-trapped interstitial is required to nucleate a new interstitial cluster.

The ballistic mixing was simulated by randomly switching two atoms according to the given distribution of the separation distance between the atoms [exponential distribution, $\exp(-R/R_0)$, with $R_0=1.08a_{\mathrm{nn}}$]. This distance was selected with guidance from molecular-dynamics simulations of energetic cascades in CuAg.[19]

The outputs of these simulations are recorded in cycles, where one cycle is 8×10^8 events per 128^3 atoms, or 381 events per atom. One event is a vacancy jump, a defect pair production event given by the rate K_0, or a ballistic mixing event given by the rate K_b. Unless otherwise stated, the results listed below represent system microstructures after 100 cycles.

III. RESULTS

A. Conditions for phase separation in ideal solid solutions of $A_{0.90}B_{0.10}$ binary alloys

Before presenting the results of the simulations, we note that within the mean-field approximation the rate equations for interstitial and vacancy populations interacting according to the rules chosen for these simulations are

$$\frac{\partial c_v}{\partial t}=\frac{\partial c_i}{\partial t}=K_0(1-f)-K_{rec}, \tag{2a}$$

$$K_{rec}=K_{iv}c_ic_v+gK_0(1-f), \quad K_{iv}=4\pi r_{iv}D_v/\Omega. \tag{2b}$$

Here, c_i and c_v are the (equal) concentrations of interstitials and vacancies, K_0 is the defect pair production rate, and K_{rec} is the defect recombination rate. The relevant defect production rate in these equations is K_0, corrected by the correlated recombination factor f, which for the conditions of these simulations is $f\approx0.66$. Due to the specifics of these simulations with instantaneously diffusing interstitials, the recombination rate K_{rec} has two separate contributions: one from the vacancy motion, proportional to the vacancy-interstitial recombination rate constant K_{iv}, and another from the interstitial motion, proportional to the defect production rate K_0. The recombination rate constant K_{iv} is a function of the recombination radius r_{iv}, the vacancy diffusion coefficient D_v, and the atomic volume Ω.[20] The factor g in Eq. (2b) denotes the probability for an interstitial to end its trajectory by recombination with a vacancy, other than its production partner, and not trapping with B atoms or clustering; g is, in general, a function of c_v. For conditions where interstitial clustering is important, c_i in Eq. (2b) should be separated into a sum of concentrations of single and clustered interstitials.

We now turn to the KMC simulations and report first our results for an $A_{0.90}B_{0.10}$ alloy system with zero ordering energy. Trapping numbers were varied from $N_{BT}=2$ to $N_{BT}=6$. The size of the simulation box is $L_0=128a_{\mathrm{nn}}$ (a_{nn} =nearest-neighbor distance). The phase-separation behavior in these alloys has been studied as a function of the defect production rate K_0. Simulations of systems with different trapping numbers N_{BT} reveal the same general pattern: below a certain defect production rate, $K_0^*(N_{BT})$, the alloy systems arrive at a state of random solution, while above it, interstitial-driven phase separation is observed. Examples of the microstructure of $A_{0.90}B_{0.10}$ alloys from simulations at rates K_0 below and above the transition rate $K_0^*(N_{BT})$, as well as the examples of different initial states used in these simulations, are illustrated in Fig. 1. Clearly, there is a distinctive difference in the morphologies between the random solution phase in Fig. 1(c) for $N_{BT}=4$ and $K_0=0.5$ s^{-1} and the two-phase morphology in Fig. 1(d) at the higher rate $K_0=5$ s^{-1}. Similar two-phase morphologies are obtained in simulations

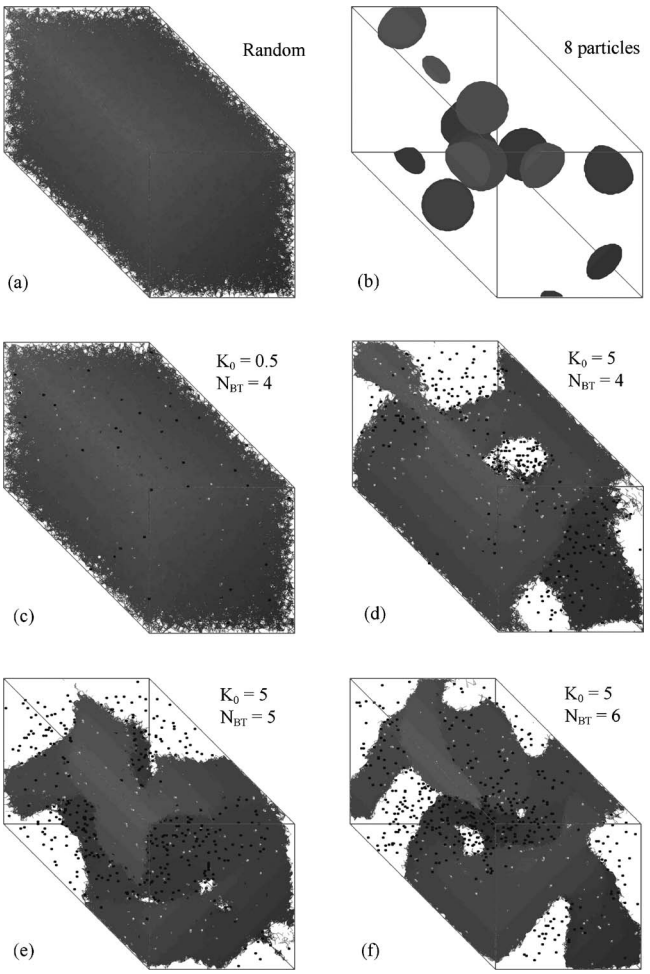

FIG. 1. Examples of (a) random solution and (b) precipitated initial states used in simulations of $A_{0.90}B_{0.10}$ alloys, and snapshots of microstructures of model systems with zero ordering energy and different production rates K_0 and trapping numbers N_{BT}: (c) $N_{BT}=4$, $K_0=0.5$ s^{-1}, (d) $N_{BT}=4$, $K_0=5$ s^{-1}, (e) $N_{BT}=5$, $K_0=5$ s^{-1}, and (f) $N_{BT}=6$, $K_0=5$ s^{-1}. Color code: precipitated *B* phase (interconnected *B*-type atoms) is shown in gray color; *A*-type matrix atoms and isolated *B*-type atoms in solution are not shown; interstitials and vacancies are shown as balls of lighter and darker colors, correspondingly. Simulation box outlined in the pictures has an orthorhombic shape.

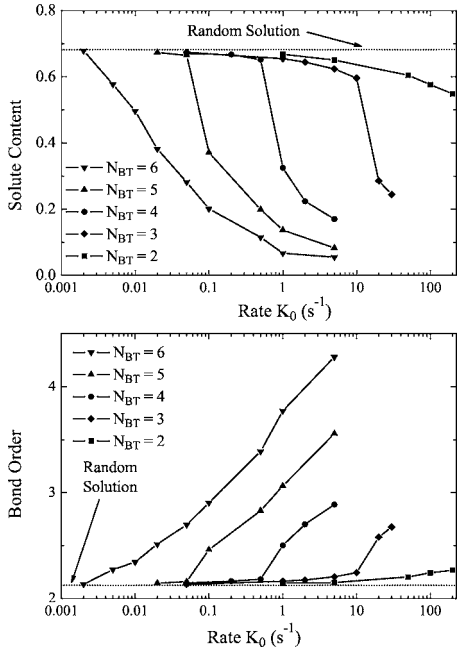

FIG. 2. Solute content (top) and bond order parameter (bottom) in $A_{0.90}B_{0.10}$ alloy systems with zero ordering energy and different trapping numbers N_{BT} as a function of the defect production rate K_0. Initial state was a random solution.

with the same defect production rate $K_0=5$ s^{-1} and larger trapping numbers $N_{BT}=5$ [Fig. 1(e)] and $N_{BT}=6$ [Fig. 1(f)]. Nearly all of the interstitials, shown as lighter-colored balls, are trapped inside the precipitates; a few clustered interstitials, however, are found outside the precipitates. The vacancies, shown as darker-colored balls in Fig. 1, have a somewhat larger tendency to be located in the solute depleted matrix, but detailed analysis shows that they are also located inside the precipitates.

The microstructure of the model systems has been characterized with the use of two variables—the average bond order (BO) parameter and the solute content (SC). The bond order parameter is defined here for a given atom as simply the average number of B-type neighbors, and the solute content represents the fraction of B atoms in solution in the matrix phase. Somewhat arbitrarily, all B atoms continuously connected in clusters of size 5 and larger are counted as the precipitated phase, while the remaining isolated B atoms and those in clusters of sizes 2, 3, and 4 atoms are counted as solute in the matrix. These definitions for the precipitated and solute phases have been used for calculations of the average bond order parameter and the solute content. For a random 10% solution, the bond order parameter is BO $=2.125$ and the solute content is SC$=0.68$. The evolution of these calculated BO and SC parameters with the defect production rate K_0 (with the data recorded after 100 cycles in simulations starting from random solutions) is shown in Fig. 2. The transition between the states of random solution and phase separation is represented by a rapid decrease of the solute content and a rapid rise of the bond order parameter in the vicinity of the transition rate $K_0^*(N_{BT})$. This transition is particularly evident from the spatial distribution of the solute concentration field, which exhibits a single peak for random

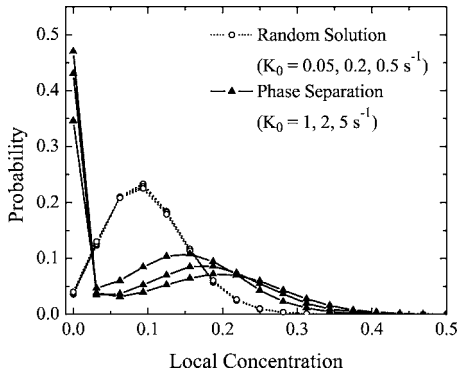

FIG. 3. Spatial distributions of solute concentration field from simulations of $A_{0.90}B_{0.10}$ alloy systems with zero ordering energy, trapping number $N_{BT}=4$, and different defect production rates K_0. The size of the unit sampling volume is 2^3 fcc cells (32 atoms).

solution and two peaks (solution and precipitated phase) for states with phase separation (see Fig. 3). The bond order parameter increases with the rate K_0 and, at sufficiently high values of K_0, it approaches a value somewhat less than the trapping number N_{BT}. N_{BT} is reasonably the upper limit for the BO parameter, since there is no driving force to bring B atoms into arrangements with more than N_{BT} of B-type nearest neighbors.

Several simulations were performed starting from a fully precipitated state represented by eight spherical pure B particles randomly positioned in the volume of the simulation box [Fig. 1(b)]. The particles have the same size, which is adjusted to yield the 10% solute phase composition. These simulations show that the initially precipitated $A_{0.90}B_{0.10}$ system tends to arrive at the same state as the simulations starting from random solutions (Fig. 4). Regardless of the initial state, therefore, the same combination of production rate K_0 and solute trapping number N_{BT} leads to the same final state: a random solution or a precipitated state. B-rich domains in the precipitated state grow until they reach dimensions com-

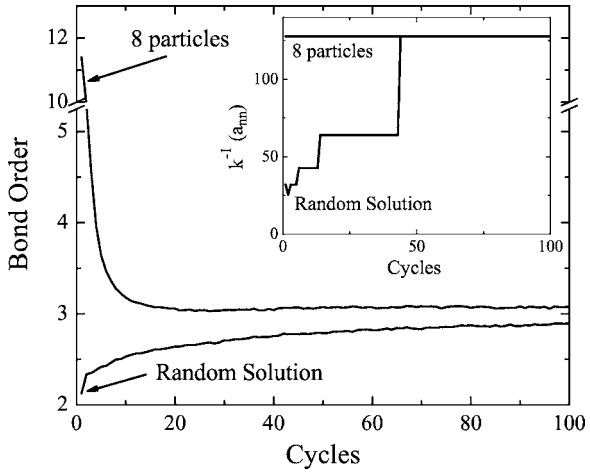

FIG. 4. Evolution of the bond order parameter in simulations of $A_{0.90}B_{0.10}$ alloy systems with trapping number $N_{BT}=4$ and defect production rate $K_0=5$ s^{-1}, starting from the random solution and fully precipitated (eight particles) states. Evolution of the structure factor is shown in the inset.

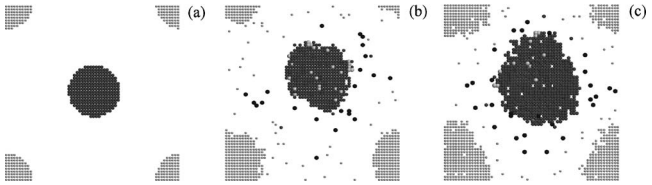

FIG. 5. KMC simulations of an isolated solute particle under irradiation: (a) initial conditions; (b) same particle, 100 KMC cycles later with $K_0=50\ s^{-1}$, and $N_{BT}=6$; (c) same as (b) but with $N_{BT}=3$. Lighter-colored atoms at the corners of the box are periodic images of the particle at the center.

parable with the size of the simulation box, indicating that the precipitating system is always in a state of macroscopic growth.

The bond order parameter of the initially precipitated structure was observed to decrease rapidly at the beginning of the irradiation and then reach its saturation value. This suggests that the initial effect of ion irradiation on the already present inclusions of B-phase particles in these systems is to induce swelling of the precipitate particles, i.e., dilution of the B concentration. The final size of the particles is determined by the steady-state values of the bond order parameter $\mathrm{BO}(K_0)$, since the bond order parameter is related to the composition of precipitates c_B as $c_B=\mathrm{BO}/z \leqslant N_{BT}/z$, where z is the lattice coordination number. This swelling effect is indeed observed in the simulations, and its magnitude increases with decreasing trapping number N_{BT} (Fig. 5).

The simulations indicate that the transition rate K_0^* decreases sharply with the trapping number N_{BT} (note the logarithmic scale of K_0 in Fig. 2). For example, the transition rate K_0^* for the $A_{0.90}B_{0.10}$ system with the highest value of the trapping number $N_{BT}=6$ is estimated to be $K_0^*(6) \approx 0.002-0.005\ s^{-1}$, while the transition rate for the $N_{BT}=3$ system is $K_0^*(3) \approx 10-20\ s^{-1}$. Simulations with $N_{BT}=2$ failed to show phase separation, even with the value of $K_0=200\ s^{-1}$. Values of K_0^* for $N_{BT}>6$ could not be determined in the present simulations, owing to limitations from the box size since the average distance traveled by interstitials in such systems begins to exceed 40 nearest-neighbor distances at this production rate, and artifacts arise from the periodic boundaries. Too small a simulation box, for example, results in an earlier onset of the random solution steady state, as demonstrated from a comparison of simulations in boxes with sizes $L_0=64a_{\mathrm{nn}}$ and $L_0=128a_{\mathrm{nn}}$. The migration range of the interstitials under all the other conditions studied in this work is small enough to ensure the adequacy of using the $L_0=128a_{\mathrm{nn}}$ simulation box.

B. Kinetic stability analysis of the random solution to macroscopic segregation transition for alloys with zero ordering energy

The observed strong dependence of the transition rate K_0^* on the trapping number N_{BT} can be understood on the basis of a simple kinetics stability analysis. There are two possible mechanisms for nucleation of solute phase particles for our ideal solution: from B-trapped and from clustered interstitials. In both cases, an immobile B-type interstitial would release the B atom onto a neighboring lattice site upon recombination prompted by an arriving vacancy and, thus, contribute to the local phase separation. This mechanism is clearly driven by kinetics rather than thermodynamics.

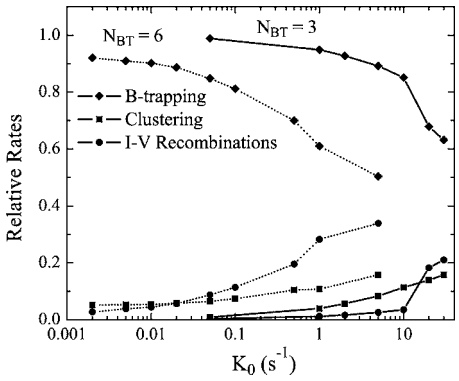

FIG. 6. Relative contributions of the three interstitial reactions (B trapping, clustering, and recombination) to the net defect production rate (K_0 minus the rate of self-recombination events) as a function of the defect production rate K_0.

The steady-state point defect concentration can be obtained from Eqs. (2a) and (2b), which in steady state becomes

$$c_{i,v}=\left[\frac{(1-g)(1-f)K_0}{K_{iv}}\right]^{1/2}. \tag{3a}$$

In the present case, the relative rates of the three interstitial reactions (B trapping, clustering, and recombination) for two representative systems with trapping numbers $N_{BT}=3$ and $N_{BT}=6$ are plotted in Fig. 6. Below the transition rate $K_0^*(N_{BT})$, the relative contributions from both the interstitial clustering and recombination reactions are small ($\leqslant 10\%$ each) compared to the trapping of interstitials in B-rich locations. Equation (3a) thus simply becomes

$$c_{i,v}=\sqrt{\frac{K_0'}{K_{iv}}}, \tag{3b}$$

where K_0' is the defect production rate corrected for correlated recombination, $K_0'=K_0(1-f)$. Indeed, the $K_0^{1/2}$ dependence of $c_{i,v}$ holds very well in the range of defect production rates used in these simulations, which varied from $K_0=0.002\ s^{-1}$ to $K_0=200\ s^{-1}$, resulting in the values of $c_{i,v}$ of $8.6\times 10^{-3}\%$ and 2.6%, respectively.

A kinetic model developed below illustrates that there is a minimum defect production rate K_0 required to induce phase separation in a given microstructure with fluctuations in the solute phase characterized by some wavelength L. The model assumes that the precipitation of B atoms into compact particles is possible only under the conditions when the time for dissolution of the nucleating particles by vacancies exceeds the time for their growth by the incoming flux of B-type interstitials. In other words,

$$\tau_v > \tau_i. \tag{4}$$

If the competing nucleation sites are separated by the average distance L, one can think of τ_v as the characteristic time required for vacancies with concentration c_v to dissolve a precipitate by homogenizing the concentration profile in the radius of length L around it:

$$\tau_v \approx L^2/(D_v c_v), \tag{5}$$

where the correlation factor for diffusion has been set equal to unity. This characteristic dissolution time should be compared with the time required for interstitials generated at rate K_0 inside the volume of a single nucleation domain to collect solute B atoms into a single precipitate:

$$\tau_i \approx c_B/K_0'. \tag{6}$$

It is assumed in Eq. (6) that in the nucleation stage, there are a sufficient number of B atoms in solution to ensure that most interstitials become B type on their way to the precipitate. From Eqs. (3)–(6), therefore, the minimum value of self-recombination corrected defect production rate $K_0^{*\prime}$ required to induce phase separation in a random solution with the average separation distance between the nucleation sites L is

$$K_0^{*\prime} = \frac{{c_B}^2 D_v \Omega}{4\pi r_{iv}} \frac{1}{L^4}. \tag{7}$$

The vacancy diffusion coefficient D_v can be estimated from the vacancy jump rate Γ, as $D_v = \Gamma/6$, with length in units of the nearest-neighbor distance a_{nn}. At $T=200\ ^\circ\mathrm{C}$ (0.040 76 eV), the jump rate is $\Gamma = 3.59 \times 10^6\ \mathrm{s}^{-1}$, yielding the value for the diffusion coefficient $D_v = 0.60 \times 10^6\ \mathrm{s}^{-1}$. Ω is on the order of unity and, for nearest-neighbor recombination, $r_{iv} \approx 1$. Thus,

$$K_0^{*\prime} = A\frac{1}{L^4} \approx 477\frac{1}{L^4}. \tag{8}$$

The same functional dependence, $\lambda^* \approx K_0^{-1/4}$, was obtained by Martin using linear stability analysis of random solutions under irradiation.[14] The critical wavelength λ^* was defined such that for a given defect production rate K_0, only fluctuations with a wavelength λ larger than λ^* are expected to grow.

As a preliminary test of Eq. (8), a series of simulations was performed, where the characteristic distance L was artificially controlled. In these simulations, the B trapping of interstitials was prevented except at sites within a certain radius away from any one of the given number of randomly positioned trapping centers. The radius of these spherical domains was adjusted to keep the total number of sites available for B trapping constant ($\approx 30\%$). Under these conditions, the characteristic distance L defining the average separation between the nucleating B-rich precipitates in Eq. (8) is the average distance between the trapping centers, $L \sim n_{tr}^{-1/3}$, where n_{tr} is the number density of the trapping centers. The alloy system in this study ($N_{BT}=4$, $K_0=0.5\ \mathrm{s}^{-1}$) was chosen since under normal conditions, i.e., with no spatial restrictions on interstitial trapping, it remains a random solution in steady state. The microstructures obtained for this system after extended times, using different numbers of trapping centers, are shown in Fig. 7. Clearly, decreasing the number of trapping centers, with the same total number of trapping sites, promotes phase separation, in agreement with the reasoning behind Eq. (7).

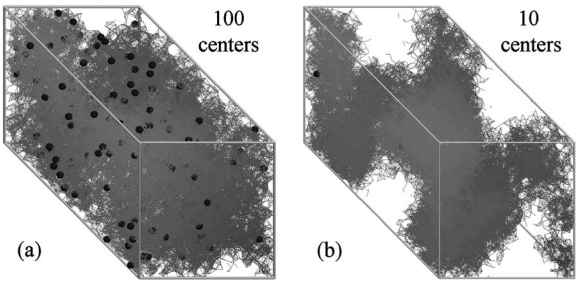

FIG. 7. Phase separation in $A_{0.90}B_{0.10}$ alloy with randomly placed (a) 100 and (b) 10 trapping centers, shown as the darker-colored balls ($N_{BT}=4$, $K_0=0.5\ \mathrm{s}^{-1}$). The total number of sites with allowed trapping is 30%. Simulation box size $L=64a_{\mathrm{nn}}$.

For homogeneous random solutions, there are no fixed trapping centers like those illustrated above; however, statistical fluctuations in solute concentration result in the presence of a number of trapping sites. The locations of these individual sites also fluctuate, but their average number density c_{NT} remains constant and defines the effective wavelength L in Eq. (7), $L \sim c_{NT}^{-1/3}$. For a perfectly random solution with trapping number N_{BT} and concentration of solute c_B, the concentration of the trapping sites is given by

$$c_{NT} = \frac{12!}{N_{BT}!(12-N_T)!} c_B^{N_{BT}} (1-c_B)^{12-N_{BT}}. \tag{9}$$

By relating the characteristic wavelength to the trapping number N_{BT} through Eq. (9), we can test Eq. (8) using the KMC results for different values of N_{BT} (Fig. 8). The open and solid symbols in Fig. 8 indicate whether irradiation with flux K_0 leads to a random solution or phase separation, respectively, while the dotted curve represents the prediction of

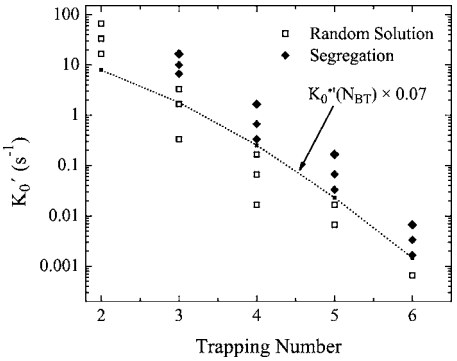

FIG. 8. The minimum defect production rate required to induce segregation in $A_{0.90}B_{0.10}$ alloys with different trapping numbers [dotted line, $K_0^*(N_{BT})$ adjusted by a factor of 0.07]. The open symbols represent random solution and the solid symbols phase separated.

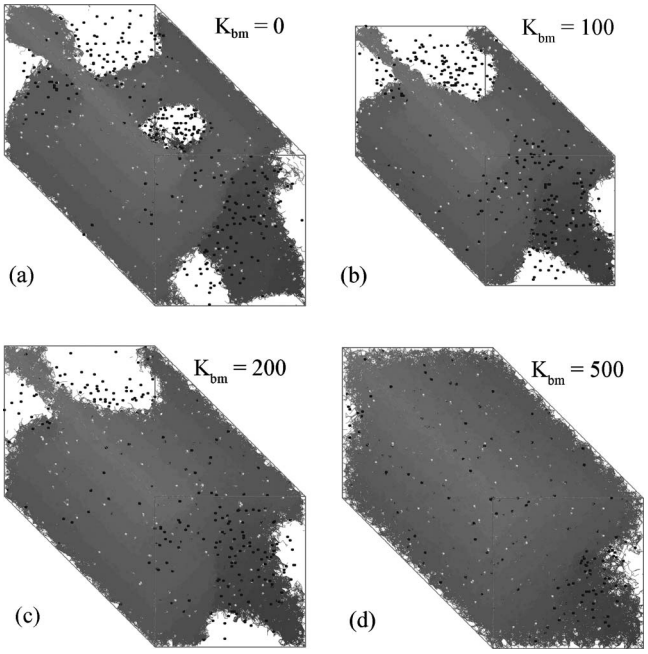

FIG. 9. The effect of ballistic mixing at different rates K_{bm} on the structure of a model $A_{0.90}B_{0.10}$ alloy system ($N_{BT}=4$, $K_0=5\ s^{-1}$): (a) 0 s^{-1}, (b) 100 s^{-1}, (c) 200 s^{-1}, and (d) 500 s^{-1}.

Eqs. (8) and (9) for the transition rate $K_0^*(N_{BT})$ adjusted by a factor of 0.07 for a better fit.

Given the approximate nature of the arguments used in the derivation of Eq. (7), the overall agreement between the model and the simulations is quite good. The relatively higher values of K_0^* observed in the simulations at low trapping numbers (at $N_{BT}=2$, phase separation did not occur even at the highest tested rate $K_0=200\ s^{-1}$) probably arise from the low B concentration in the precipitated particles [see Fig. 2(b)] since the precipitates then occupy a large fraction of the alloy volume and this effectively decreases the wavelength L.

C. Effect of ballistic mixing

Irradiations with energetic ions or fast neutrons result not only in the enhanced defect production but also in ion-beam (ballistic) mixing.[21] It has been shown in recent studies that the introduction of such mixing in an alloy can significantly alter its phase diagram.[22] For example, compositional patterning in some irradiated alloys has been observed.[23,24] Interstitial transport of solute, however, was not expected in these cases. Here, we consider the effect of ballistic mixing on the microstructure of model $A_{0.90}B_{0.10}$ ideal solution, but now for the case where solute transport occurs predominantly by an interstitial mechanism. We employ a system with trapping number $N_{BT}=4$ and defect production rate $K_0=5\ s^{-1}$ for demonstration. The results of these simulations are shown in Fig. 9.

The addition of ballistic mixing has led to the eventual formation of the random solution state at a sufficiently high ballistic mixing rate $K_{bm}\approx 500\ s^{-1}$. The ratio of K_{bm}/K_0 at this mixing rate is 100, which is typical for heavy-ion irradiations of many metals.[21] None of the microstructures showed evidence of patterning, i.e., stabilization of the size of precipitates at some constant value below the size of the simulation box. This result is not unexpected here, since patterning derives from a competition between ordering (interstitial migration) and disordering (ballistic mixing) mechanisms.[18] In the present model, the former mechanism is scale independent, whereas the latter becomes less efficient at longer length scales, so that a system with few large precipitates is statistically more stable than a system with many small precipitates. The sole effect of ballistic mixing, therefore, is analogous to the randomizing effect of vacancy diffusion and should be incorporated accordingly into the model by contributing to shorter characteristic dissolution times in Eq. (5).

D. Effect of nonzero ordering energy

1. Case with solute trapping of interstitials: $N_{BT}\leqslant z$

In an alloy with a nonzero ordering energy, vacancies are no longer chemically neutral and exhibit an increasing asymmetry for exchanges with increasing ordering energy. Thus, the effect of vacancies on the microstructure of such alloys cannot be captured by the simple randomization described by Eq. (5) and the expression for the critical defect production rate K_0^* does not hold. In order to elucidate the behavior of such alloys with nonzero ordering energies, a set of simulations was performed for the same representative system defined by a trapping number $N_{BT}=4$ and a defect production rate $K_0=5\ s^{-1}$ at temperature $T=200\ ^\circ C$ ($k_BT=0.040\ 76$ eV). The ordering energies of model alloys in this study varied from -0.05 to $+0.05$ eV. For convenience, the ordering energy ω will be given in dimensionless units of ω/k_BT in what follows.

Representative snapshots of the microstructures obtained in these simulations are shown in Fig. 10. These images suggest that there exists a distinctive morphological transition between the microstructures of $A_{0.90}B_{0.10}$ alloys with $\omega\leqslant\omega_1$, $\omega_1\approx 0.25$ and $\omega\geqslant\omega_2$, $\omega_2\approx 0.75$. In the case of small ordering energies, below ω_1, alloys develop interconnected domain structures characteristic of the interstitial-driven precipitation [Figs. 10(a) and 10(b)]. For the ordering energies above ω_2, the alloys exhibit phase decomposition similar to that expected from the vacancy-driven thermal precipitation, i.e., compact solute-rich particles [Fig. 10(d)]. Recall that the microstructure in Fig. 10(d) is recorded after 100 cycles and does not represent a steady state; the precipitates are still growing. Finally, and somewhat unexpectedly, alloys with an intermediate value of the ordering energy, $\omega=0.50$, developed a random solution structure [Fig. 10(c)].

The three observed modes of the evolution of alloy microstructure (interstitial-driven precipitation, random solution, and vacancy-driven precipitation) can be characterized by the dependences of the solute content and bond order parameter on the ordering energy (Fig. 11). Their presence is also evident from the spatial distributions of local solute concentrations (Fig. 12). In particular, the random solution structure at intermediate ordering energies is indicated by the sharp peak in solute concentration at $\omega=0.50$. At lower

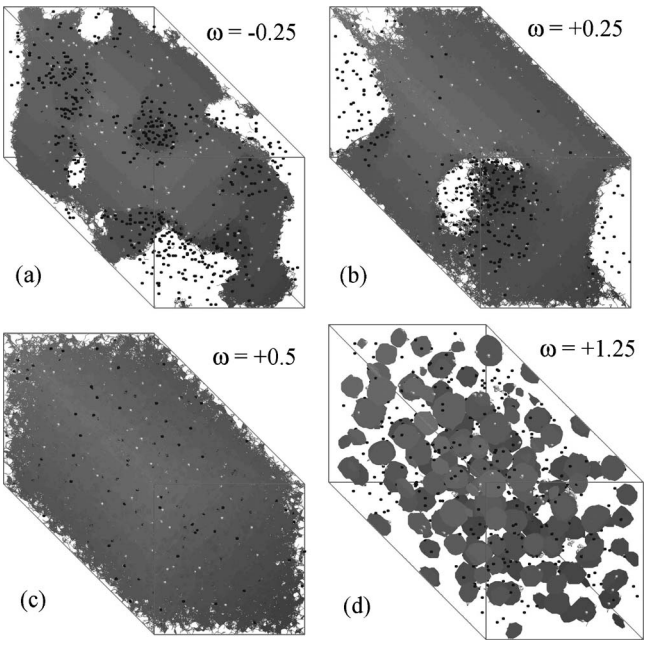

FIG. 10. The effect of ordering energy ω on the structure of a model $A_{0.90}B_{0.10}$ alloy system ($N_{BT}=4$, $K_0=5\ s^{-1}$). Simulation box size is $L=128a_{nn}$; $k_BT=0.040\ 76$ eV.

values of ω, the bond order parameter remains at a value BO$\approx$3, characteristic of loose precipitates formed by interstitial-driven aggregation, while at the higher values of ω, the bond order parameter reaches BO$\approx$11, which is characteristic of compact *B*-rich particles preferentially formed by vacancy motion. Clearly, there exists a competition between the interstitial- and vacancy-driven modes of growth in the studied alloy systems with nonzero ordering energies, which results in a structural frustration at $\omega=0.50$ (0.02 eV). For this value of ω, which yields a critical temperature of 318 °C, the solubility limit at 200 °C just equals 10 at. %. We can understand the formation of a solid solution near $\omega=0.50$, therefore, by noting that the short-range order will increase rapidly with increasing ordering energy at this value of ω. As a consequence, the number of trapping sites also rapidly increases and the characteristic distance L between

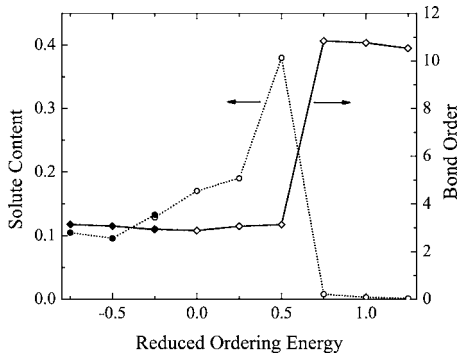

FIG. 11. Solute content and bond order parameter in $A_{0.90}B_{0.10}$ alloy systems as functions of the ordering energy ω. $N_{BT}=4$, $K_0=5\ s^{-1}$ simulations in $L=64a_{nn}$ (solid symbols) and $L=128a_{nn}$ (open symbols) boxes.

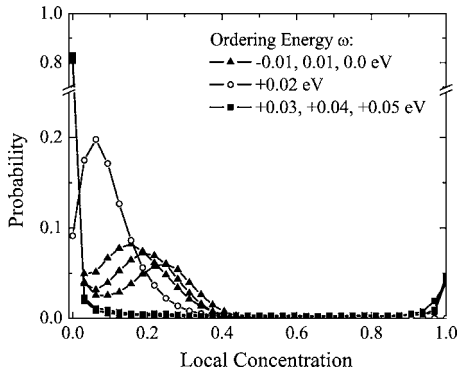

FIG. 12. Spatial distributions of solute concentration field from simulations of $A_{0.90}B_{0.10}$ alloy systems with trapping number $N_{BT}=4$ and defect production rates $K_0=5\ s^{-1}$, for different ordering energies ω. The size of the unit sampling volume is 2^3 fcc cells (32 atoms).

the nucleation sites decreases. According to Eq. (8), this results in higher values of K_0 necessary to trigger interstitial-driven nucleation.

We also considered briefly a system for which $\omega\approx-1$ (Fig. 13). In this case, the number of *B*-*B* bonds is reduced, so that trapping centers become sparse. As a consequence, interstitials transport solute to a few nucleation sites which grow with a very porous structure. Vacancies, on the other hand, disrupt the solute network. In steady state, the morphology becomes a quasirandom solution with small interconnected solute precipitates formed around clustered interstitials.

2. Case with no solute trapping of interstitials: $N_{BT}>z$

If the number of nearest neighbor solute atoms required to trap an interstitial, N_{BT}, is set larger than the coordination number z, interstitials can no longer be trapped by solute, and they must either recombine with vacancies or join inter-

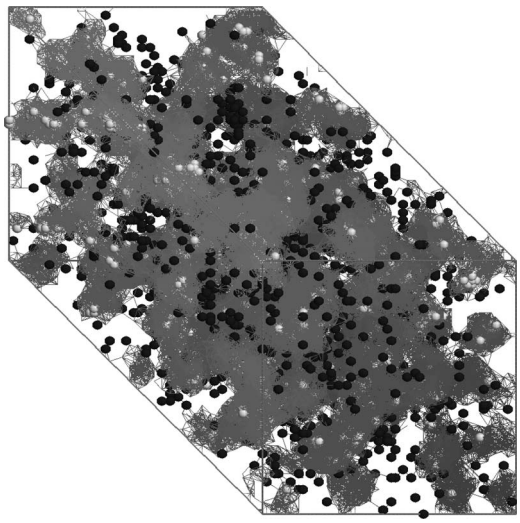

FIG. 13. Quasirandom solution microstructure of a model $A_{0.90}B_{0.10}$ alloy system ($N_{BT}=4$, $K_0=5\ s^{-1}$) with the ordering energy ω, $\omega=-k_BT$. Simulation box size is $L=64a_{nn}$; $k_BT=0.040\ 76$ eV.

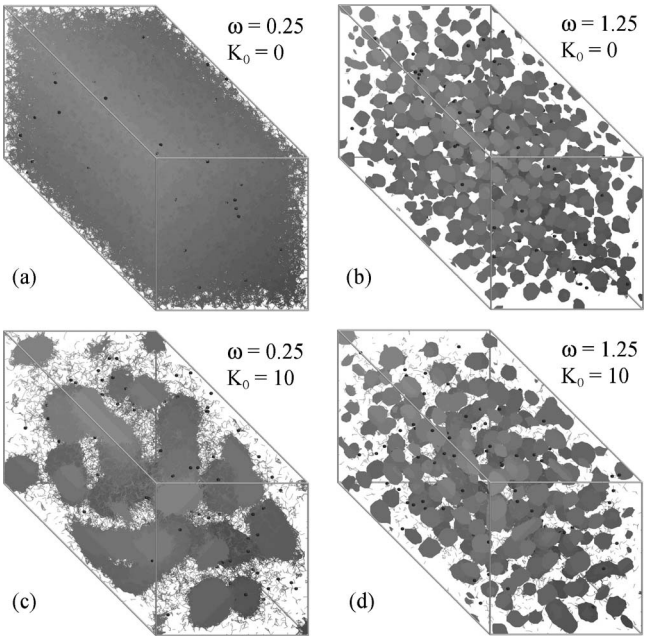

FIG. 14. The effect of nonzero ordering energy ω on the structure of a model $A_{0.90}B_{0.10}$ alloy system with (B_{NT}=14, K_0=10 s^{-1}) and without (K_0=0 s^{-1}) defect pair production. Simulation box size is $L=128a_{nn}$; k_BT=0.040 76 eV.

stitial clusters. While interstitials might still be capable of transporting solute atoms in our model, the sites where interstitial-vacancy recombination occurs are not preferentially located at solute-rich areas, since in an ideal solution, vacancies undergo random-walk motion. The alloy, therefore, remains in a state of random solution. In alloys with a positive heat of solution, on the other hand, vacancies tend to occupy lattice sites in solute-rich areas. This results in establishing point defect and solute fluxes to these regions, and precipitates can nucleate.

Several simulation runs were performed on such systems with no trapping of interstitials, using a constant rate of defect production (K_0=10 s^{-1}). Interstitial clustering was suppressed in these simulations by initiating them with 100 randomly placed vacancies. Thus, production of each vacancy-interstitial pair could result only in a recombination reaction, maintaining the initial number of point defects constant throughout the simulations. The same size of the simulation box ($L=128a_{nn}$) and temperature (k_BT=0.040 76 eV) were used as before, and the reduced ordering energy was varied between 0.25 and 1.25. For comparison, corresponding runs in the absence of defect production (K_0=0 s^{-1}) were also completed. These latter runs represent solute precipitation in a system containing only vacancies. It can be seen from the snapshots of alloy microstructures in Fig. 14 that the introduction of the solute-carrying interstitials in the system has, indeed, resulted in an enhancement of phase separation. At the ordering energy ω=0.25, the annealed alloy remains in a state of random solution, whereas the irradiated alloy exhibits solute segregation in the form of compact precipitates. We note that this case is similar to Al-Zn for which irradiation-induced homogeneous precipitation was proposed by Cauvin and Martin in Ref. 15. These authors showed that the solubility limit under irradiation, c_{irr}, is given approximately by the expression

$$c_{irr} = c_{eq}\left[1 + \frac{D_s^i}{D_s^v}\right]^{-1}, \tag{10}$$

where D_s^j represents the solute diffusion coefficient arising from interstitial or vacancy mechanisms. Since $D_s^i \gg D_s^v$ in our system, $c_{irr} < c_{eq}$ and precipitation takes place. For ω =1.25, both the unirradiated and irradiated alloys exhibit similar structures, although the growth of precipitates in the irradiated alloy proceeds faster, owing to the assistance of the interstitial diffusion mechanism.

IV. SUMMARY AND CONCLUSIONS

This work has explored the role of radiation-induced interstitials on alloy stability in $A_{0.90}B_{0.10}$ alloys. It complements previous KMC simulations that have considered the competition between ion-beam mixing and radiation-induced diffusion promoted solely by vacancies in simple eutectic alloys. In the first part of this work, the question of defining the necessary conditions for such interstitial-promoted homogeneous nucleation was addressed for the particularly simple case of ω=0 eV, i.e., the case of chemically indifferent vacancies diffusing according to a random-walk pattern. A simple kinetic model was proposed, in which the interstitial-promoted growth rate is compared with the dissolution rate from vacancies to find the critical defect production rate K_0^*, above which phase separation occurs and below which the alloy remains in a state of random solution. The model stipulates that the rate K_0^* is proportional to the inverse of the fourth power of some characteristic distance L, which is the average distance between the potential nucleation centers. In our model ideal solution, the nucleation centers are associated with the interstitial traps, i.e., lattice points with more than N_{BT} nearest-neighbor solute atoms. The resulting exponential dependence of the rate K_0^* on the number N_{BT} is well reproduced by the simulations.

The case of alloys with a nonzero ordering energy was considered in the second part of this work. In particular, a transition between the interstitial-driven and vacancy-driven (thermal ripening type) modes of phase separation was observed to occur at $\omega_{tr} \sim k_BT/2$ upon increasing the ordering energy from slightly negative values. The two types of phase separation are drastically different with respect to the morphology and density of the solute precipitates. Solute precipitates from the interstitial-driven growth develop into continuous percolating domains with the solute content $\sim N_{BT}/z$, while precipitates from the vacancy-driven growth are characterized by compact spherical shapes with very small admixture of matrix atoms. Unexpectedly, a state of random solution was observed in the vicinity of the transition point at ω_{tr}. It was argued that increasing the ordering energy causes the creation, from the correlated vacancy motion, of an increasing number of interstitial trapping sites in excess of those found in an ideal random solution. Consequently, the characteristic distance L between the nucleation sites decreases, eventually making interstitial-driven nucleation im-

possible. At the same time, the entropy of the system with $\omega=\omega_{tr}$ remains high enough to preclude phase separation via the usual vacancy-driven precipitation (ω_{tr} corresponds to the thermodynamic solubility limit of the model 10% alloy).

We also considered the case in which interstitials perform only a solute transport function. In these simulations, the trapping number N_{BT} was set to a number above the coordination number z so that the trapping of interstitials in solute-rich locations became impossible. In contrast to the case of zero ordering energy considered above, recombination of the migrating interstitials with vacancies rather than with migrating vacancies on the immobile trapped interstitials could possibly lead to phase separation in alloys with a positive ordering energy in this case. Although in the absence of irradiation alloys with a slightly positive ordering energy, $0<\omega<\omega_{tr}$, remain in a state of random solution, more local solute-rich sites are created by vacancies than in an ideal solution with $\omega=0$. Also, vacancies tend to spend more time at these locations jumping back and forth from solute atoms. Consequently, recombination of solute-type interstitials at vacancies in such alloys may provide the required directionality to the flux of solute atoms and induce phase separation. Realization of such a scenario was indeed observed in our simulations where phase separation of the interstitial-driven type was observed for alloys with $\omega<\omega_{tr}$.

Lastly, we comment on the relevance of these simulations to real systems. In some cases, the displacement rate K_0 required for precipitation in our study exceeded 1 s^{-1}, which of course far exceeds those in nuclear reactor environments, or even ion-beam irradiations. Values for $N_{BT}=6$, on the other hand, are close to displacement rates during ion-beam irradiations. Equation (8) shows, moreover, that K_0 scales as L^4. We have employed 10% alloys to keep L from becoming too large. In 1% alloys, however, L increases by a factor of ≈ 100 [see Eq. (9)] and K_0 is reduced by a factor of $\approx 10^8$. We have also assumed in our model system that the interstitial atoms are completely trapped in certain specific environments. For the types of behavior observed, however, it is probably sufficient that the trapping reduces interstitial mobility to a value less than that of the vacancy. Otherwise, the mobile interstitial-solute complex would migrate to the vacancy and annihilate at random locations. Systems that may show the effects found here and presently of interest for structural components in reactors are Fe-rich Fe-Cr and Fe-Cu. For Fe-Cr, it has been argued from recovery experiments that mixed dumbbell interstitials are slightly more mobile than self-interstitials and that the mixed dumbbells trap at Cr solute atoms.[25] For very dilute Fe-Cu alloys, atom-probe studies of irradiated alloys have shown that Cu forms "dilute" precipitates or clusters that contain large amounts of Fe.[26] This finding may be an indication of the porous structure observed here. Finally, we mention Ni-rich Ni-Cu alloys. Our molecular-dynamics simulations using embedded atom potentials indicate that diffusion of Cu by mixed dumbbells is much larger than diffusion of Ni-Ni dumbbells and that trapping of interstitials in regions of high Cu content takes place,[27] thus making them susceptible to the interstitial-driven porous precipitation discussed here.

ACKNOWLEDGMENTS

This work was supported by the U.S. Department of Energy, Division of Materials Sciences under Grant No. DE-FG02-05ER46217 and the NSF under Grant No. DMR04-07958.

[1] See, e.g., *Fundamentals of Radiation Damage*, edited by I. M. Robertson, R. S. Averback, D. K. Tappin, and L. E. Rehn (North-Holland, Amsterdam, 1994).
[2] J.-L. Bocquet and G. Martin, J. Nucl. Mater. **83**, 186 (1979).
[3] K. C. Russell, J. Nucl. Mater. **83**, 176 (1979).
[4] G. Silvestre, A. Silvent, C. Regnard, and G. Sainfort, J. Nucl. Mater. **57**, 125 (1975).
[5] A. Barbu and A. J. Ardell, Scr. Metall. **9**, 1233 (1975).
[6] P. R. Okamoto, A. Taylor, and H. Wiedersich, U.S. ERDA Conference, 1975, edited by M. T. Robinson and F. W. Young (unpublished), Paper No. 751006, p. 1188.
[7] P. R. Okamoto and H. Wiedersich, J. Nucl. Mater. **53**, 336 (1974).
[8] R. Cauvin and G. Martin, J. Nucl. Mater. **83**, 67 (1979).
[9] W. Wagner, R. Poerschke, A. Axmann, and D. Schwahn, Phys. Rev. B **21**, 3087 (1980).
[10] T. R. Anthony, AEC Symposium, 1972, edited by J. W. Corbett and L. C. Ianniello (unpublished), Paper No. 701601, p. 630.
[11] A. Barbu, Acta Metall. **28**, 499 (1980).
[12] R. A. Johnson and N. Q. Lam, Phys. Rev. B **13**, 4364 (1976); **15**, 1794 (1977).
[13] F. Soisson, Philos. Mag. **85**, 489 (2005).
[14] G. Martin, Phys. Rev. B **21**, 2122 (1980).
[15] R. Cauvin and G. Martin, Phys. Rev. B **23**, 3322 (1981).
[16] P. R. Okamoto and L. E. Rehn, J. Nucl. Mater. **83**, 1 (1979).
[17] R. S. Averback and P. Ehrhart, J. Phys. F: Met. Phys. **14**, 1347 (1984).
[18] Raul A. Enrique and Pascal Bellon, Phys. Rev. B **63**, 134111 (2001).
[19] K. Nordlund, J. Tarus, J. Keinonen, M. Ghaly, and R. S. Averback, Nucl. Instrum. Methods Phys. Res. B **164-165**, 441 (2000).
[20] R. Sizmann, J. Nucl. Mater. **69/70**, 386 (1978).
[21] R. S. Averback and T. Diaz de la Rubia, Solid State Phys. **51**, 282 (1998).
[22] G. Martin, Phys. Rev. B **30**, 1424 (1984).
[23] Raúl A. Enrique and Pascal Bellon, Phys. Rev. Lett. **84**, 2885 (2000).
[24] P. Krasnochtchekov, R. S. Averback, and P. Bellon, Phys. Rev. B **72**, 174102 (2005).
[25] F. Maury, P. Lucasson, A. Lucasson, F. Faodo, and J. Bigot, J. Phys. F: Met. Phys. **17**, 1263 (1987).
[26] P. Pareige, B. Radiguet, and A. Barbu, J. Nucl. Mater. **352**, 75 (2006).
[27] A. Webster, P. Krasnochtchekov, and R. S. Averback (unpublished).